

# Comparison of toughness propagation criteria for blade-like and pseudo-3D hydraulic fractures



E.V. Dontsov<sup>a,\*</sup>, A.P. Peirce<sup>b</sup>

<sup>a</sup> Department of Civil and Environmental Engineering, University of Houston, Houston, TX, USA

<sup>b</sup> Department of Mathematics, University of British Columbia, Vancouver, B.C., Canada

## ARTICLE INFO

### Article history:

Received 2 November 2015

Received in revised form 6 April 2016

Accepted 11 April 2016

Available online 20 April 2016

### Keywords:

Hydraulic fracturing

PKN model

Pseudo-3D model

Non-local elasticity

## ABSTRACT

The goal of this study is to compare and evaluate the accuracy of different approaches to incorporating the effect of lateral fracture toughness into reduced models for blade-like and pseudo-3D hydraulic fractures. The following three methods are used for the comparison: (i) a classical model with a plane strain (or local) elasticity assumption and a pressure boundary condition calculated based on energetic considerations, (ii) a classical model with local elasticity and pressure boundary condition originating from “stitching” a radial fracture tip to the rest of the fracture, and (iii) a novel model with non-local elasticity and a boundary condition at the tip that is consistent with the linear elastic fracture mechanics propagation criterion. Predictions of all three approaches are compared to a reference solution calculated using a fully planar hydraulic fracturing simulator. The results indicate that the reduced model with non-local elasticity is able to provide an accurate approximation for a wide range of fracture toughness values. The models that feature the local elasticity assumption are able to provide reasonably accurate results for moderate values of fracture toughness, while they become less accurate for blade-like geometries and significantly less accurate (and in some cases unstable) for the pseudo-3D geometry for large values of the fracture toughness.

© 2016 Elsevier Ltd. All rights reserved.

## 1. Introduction

The ability to model a propagating hydraulic fracture is an essential tool for designing a hydraulic fracture treatments. Multiple approaches can be employed. For instance, the fracture geometry can be straight or curved in plane strain elastic conditions [1,2], penny-shaped (radial) [3], planar [4,5], or a system of fractures [6,7] can be analyzed. This study focuses solely on the propagation of planar vertical hydraulic fractures. In particular, two fracture geometries are considered, namely the Perkins–Kern–Nordgren (PKN) [8,9] (or blade-like) fracture geometry and pseudo-3D (P3D) [10–13] fracture geometry with symmetric stress barriers. Both PKN and P3D models are reduced models, since they use a series of approximations that reduce the complexity (and dimensionality) of the problem, making the resulting method computationally efficient. In the original formulations, however, both the PKN and P3D models lack a toughness propagation criterion in the lateral direction, which causes significant discrepancies in situations when fracture toughness is dominant. Several improvements have been made to account for the effect of fracture toughness. This paper aims to summarize and evaluate the accuracy of the available approaches for both PKN and P3D fracture geometries.

\* Corresponding author.

E-mail address: [edontsov@central.uh.edu](mailto:edontsov@central.uh.edu) (E.V. Dontsov).

## Nomenclature

$x, y, z$	spatial coordinates
$t$	time
$H$	height of the reservoir layer
$h(x, t)$	fracture height
$l(t)$	fracture half-length
$\Delta\sigma$	magnitude of stress barriers
$w$	fracture width
$\bar{w}$	effective width
$E' = E/(1 - \nu^2)$	plane strain Young's modulus
$p$	fluid pressure
$K_{Ic}$	fracture toughness
$\mu' = 12\mu$	scaled fluid viscosity
$Q_0$	inlet flux
$\bar{q}_x$	vertically-averaged fluid flux
$U_{ps}$	elastic energy density in plane strain
$G_c$	fracture energy per unit area

The PKN model considers a vertical planar hydraulic fracture that propagates laterally, while the fracture height is constant throughout the fracture. This situation occurs when a reservoir layer is surrounded by two impenetrable layers that arrest the fracture propagation in the vertical direction. Due to the elongated shape of the fracture, plane strain elastic conditions prevail in each vertical cross-section (away from fracture tip), and the fluid flow is predominantly horizontal. The latter implies that the pressure is constant in each vertical cross-section, which, together with the plane strain (or so-called local) elasticity assumption, leads to the conclusion that each fracture cross-section has an elliptical shape. The knowledge of the fracture width profile in the vertical direction permits one to formulate the problem in terms of a vertically-integrated lubrication equation, which reduces the dimension of the problem and makes the model computationally efficient. Clearly, the model assumptions are violated near the fracture tip, since the plane strain elasticity assumption does not hold near the fracture tip region. In situations when a PKN fracture propagates in the viscous regime (viscous dissipation dominates), the fracture tip region does not have a significant influence on the solution since viscous dissipation is distributed throughout the fracture. However, when a PKN fracture propagates in the toughness regime (fracture energy dissipation dominates), the fracture tip region has a substantial impact since the fracture energy is dissipated at the fracture tip. For this reason, the original formulation of the PKN model is not able to capture effect of fracture toughness accurately. One correction has been proposed by Nolte [14], in which a pressure boundary condition at the tip is used to capture the effect of fracture toughness. The value of the latter pressure is taken from the solution for a uniformly pressurized penny-shaped fracture, whose diameter is equal to the fracture height. In this approach half of the radial fracture that resembles the fracture tip is “stitched” to the rest of the fracture. Another approach has been recently introduced in [15], in which a different pressure boundary condition has been proposed. The approach utilizes energy considerations, for which the elastic energy release rate (calculated assuming plane strain elasticity in each vertical cross-section) is equated to the fracture energy required to break the rock ahead of the fracture tip. The difference between two proposed values for the pressure boundary condition is approximately 10%. A qualitatively different approach to capture the effect of fracture toughness has been suggested in [16], where the local elasticity assumption has been replaced by non-local elasticity (with a suitable propagation criterion that is consistent with linear elastic fracture mechanics), which remains valid even near the fracture tip. The results in [16] are presented for a pseudo-3D fracture geometry and demonstrate an excellent agreement with the reference solution even for large values of fracture toughness. Since the results in [16] do not consider the PKN fracture geometry, this study aims to describe an analogous formulation with non-local elasticity for the PKN fracture geometry, and to compare its performance to the existing corrections for the effect of fracture toughness [14,15] and a reference solution. It should be noted here that the analysis of the non-local elasticity equation for the PKN fracture was first done in [17], while no numerical results for a PKN model with non-local elasticity and coupled fluid dynamics were presented.

The classical pseudo-3D (P3D) model with symmetric stress barriers [13] is an extension of the PKN model, where a vertical fracture growth is allowed. Similar to the PKN fracture, the P3D model assumes a uniform pressure in each vertical cross-section and uses plane strain (or local) elasticity to obtain a solution for the vertical fracture width profile. The primary difference comes from the presence of stress barriers, which introduce an additional compressive stress in the layers above and below the reservoir layer. Note that the values of the elastic constants are assumed to be identical in all layers. The stress barriers change the elliptical shape of the fracture width cross-section (for a PKN fracture) to a more complicated shape, which is given by an analytical function. As for the PKN model, the governing equation for a P3D fracture is a vertically-averaged lubrication equation, in which case the computations are reduced to solving a one-dimensional problem making the P3D model extremely computationally efficient. Since the plane strain elasticity assumption becomes invalid near the fracture tip (as for a PKN fracture), a P3D model is unable to accurately capture the effect of fracture toughness (as the

original PKN model). One possibility is to use a pressure boundary condition at the fracture tip stemming from “stitching” of a half of a penny-shaped fracture, as proposed by [14]. Another option is to calculate the pressure boundary condition based on the energy considerations [15], but to generalize the developments to a P3D fracture geometry. Finally, one can use the enhanced pseudo-3D (EP3D) model [16], which uses a non-local elasticity together with a suitable propagation criterion to capture the effect of fracture toughness. In order to evaluate the performance of all three approaches, this study aims to compare the predictions of different approaches to a reference solution for large values of fracture toughness.

This paper is organized as follows. Section 2 describes and compares various approaches to capture the effect of fracture toughness for the PKN fracture geometry. Section 3 provides a similar description and comparison for the P3D fracture geometry. Finally, Section 4 summarizes the results. It should be noted that all computations presented in this paper assume no leak-off.

## 2. Comparison of toughness propagation criteria for a blade-like (PKN) hydraulic fracture

### 2.1. PKN model with local elasticity and a pressure boundary condition

This section describes governing equations that describe propagation of a PKN fracture. Schematics of a PKN hydraulic fracture is shown in Fig. 1, where  $z$  denotes the vertical axis,  $x$  the horizontal axis, while fracture opening is depicted in the  $y$  direction. Following the assumptions of the PKN model, fracture height growth is not permitted, in which case the footprint is solely contained in the reservoir layer with height  $H$  and the fracture tip is flat. The fracture propagates in the horizontal direction  $x$ , its half-length is denoted by  $l$ , while the source is located at the origin, i.e.  $x = 0$ . Each vertical cross-section in a PKN fracture is elliptic, and the pressure is determined based on plane strain elastic conditions. This implies that

$$w(x, z) = \frac{4}{\pi} \bar{w} \sqrt{1 - \left(\frac{2z}{H}\right)^2}, \quad p(x) = \frac{2E' \bar{w}}{\pi H}, \quad \bar{w}(x) = \frac{1}{H} \int_{H/2}^{H/2} w dz, \tag{1}$$

where  $w$  denotes fracture opening,  $\bar{w}$  is the effective width,  $p$  is the fluid pressure,  $E' = E/(1 - \nu^2)$  is the plane strain Young’s modulus, and  $H$  is the height of the reservoir layer. In the absence of leak-off, as considered in this study, the vertically-integrated lubrication equation is

$$\frac{\partial \bar{w}}{\partial t} + \frac{\partial \bar{q}_x}{\partial x} = \frac{Q_0}{H} \delta(x), \quad \bar{q}_x = -\frac{1}{H \mu'} \frac{\partial p}{\partial x} \int_{-H/2}^{H/2} w^3 dz = -\frac{12 \bar{w}^3}{\pi^2 \mu'} \frac{\partial p}{\partial x}, \tag{2}$$

where  $\mu' = 12\mu$  is the scaled fluid viscosity. Here the expression for the flux  $\bar{q}_x$  arises from Poiseuille flow for a Newtonian fluid in a channel. Eqs. (1) and (2) can be combined to yield

$$\frac{\partial \bar{w}}{\partial t} - \frac{6E'}{\pi^3 \mu' H} \frac{\partial^2 \bar{w}^4}{\partial x^2} = \frac{Q_0}{H} \delta(x), \tag{3}$$

which is the governing equation for a PKN model.

In order to solve (3), one needs to specify an appropriate boundary condition at the fracture tip. The classical PKN model is complemented by a zero fracture opening condition at the fracture tip, i.e.  $\bar{w}(l) = 0$ . This boundary condition, however, does not account for the effect of lateral fracture toughness. Recently, a different boundary condition, which accounts for the effect of fracture toughness, has been proposed in [15]. This condition is based on energy considerations and can be written as

$$p_E(l) = \frac{2K_{Ic}}{\sqrt{\pi H}}, \tag{4}$$

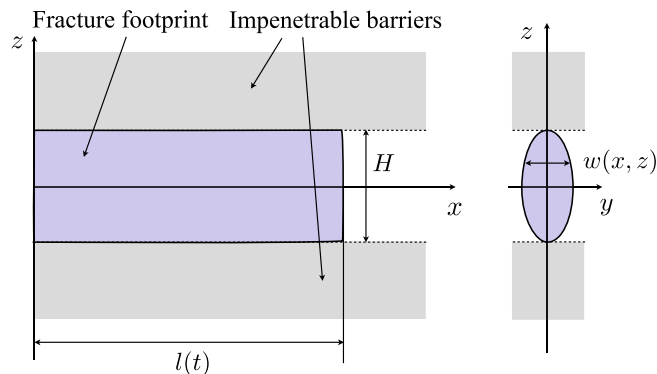


Fig. 1. Schematics of a PKN fracture.

where  $K_{Ic}$  is the fracture toughness of the reservoir layer. Here the subscript “E” indicates that the boundary condition is calculated based on energy considerations. There is an alternative to (4) proposed earlier by [14], in which the pressure that corresponds to a radial fracture with the diameter  $H$  is used for the boundary condition, namely

$$p_R(l) = \sqrt{\frac{\pi}{2H}} K_{Ic}. \tag{5}$$

Here the subscript “R” indicates that the radial (or penny-shaped) fracture is used to determine pressure boundary condition. Eqs. (4) and (5) can be rewritten using (1) as

$$\bar{w}_E(l) = \frac{\sqrt{\pi H} K_{Ic}}{E'}, \quad \bar{w}_R(l) = \left(\frac{\pi}{2}\right)^{3/2} \frac{\sqrt{H} K_{Ic}}{E'}. \tag{6}$$

In order to obtain a solution for a PKN fracture, the governing Eq. (3) is solved numerically in conjunction with one of the boundary conditions from (6). The details of the numerical scheme are omitted for brevity.

### 2.2. PKN model with non-local elasticity

Despite the fact that the PKN model described in Section 2.1 has a correction for the lateral fracture toughness (implemented through one of the boundary conditions in (6)), the local elasticity assumption is not valid near the fracture tip, in which case the near-tip behavior may not be captured accurately. To overcome this problem, this section describes a PKN model which accounts for non-local elastic interactions. The PKN model with non-local elastic interactions that is considered in this section is a reduction of the enhanced pseudo-3D (EP3D) model [16], and for this reason is referred here as the enhanced PKN model (EPKN).

The underlying idea behind implementing the non-local elastic interactions [17] is to replace the pressure-width relation in (1) with the two-dimensional elasticity integral that is used for fully planar fractures (see e.g. [5]), and to substitute the elliptic fracture opening from (1) to obtain

$$\begin{aligned} p(x) &= -\frac{E'}{8\pi} \int_{-l(t)}^{l(t)} \int_{-\frac{1}{2}H}^{\frac{1}{2}H} \frac{w(x', z') dz' dx'}{((x' - x)^2 + z'^2)^{3/2}} = -\frac{E'}{2\pi^2} \int_{-l(t)}^{l(t)} \bar{w}(x') \left[ \int_{-\frac{1}{2}H}^{\frac{1}{2}H} \frac{\sqrt{1 - (2z'/H)^2} dz'}{((x' - x)^2 + z'^2)^{3/2}} \right] dx' \\ &= -\frac{2E'}{\pi^2 H} \int_{-l(t)}^{l(t)} \bar{w}(x') \frac{dG(2(x' - x)/H)}{dx'} dx', \end{aligned} \tag{7}$$

where the kernel  $G(\cdot)$  is

$$G(s) = \frac{\sqrt{1+s^2}}{s} E\left(\frac{1}{1+s^2}\right), \quad G(s) \approx \frac{\pi}{2} \text{sign}(s), \quad |s| \gg 1, \quad G(s) \approx \frac{1}{s}, \quad s \ll 1, \tag{8}$$

and  $E(m) = \int_0^{\pi/2} (1 - m \sin^2 \theta)^{1/2} d\theta$  is the complete elliptic integral of the second kind. The elasticity Eq. (7) is a replacement for the local elasticity equation in (1), while the governing lubrication Eq. (2), and the elliptical vertical cross-section assumption remain the same.

In order to introduce the effect of fracture toughness, one should also specify a proper boundary condition (or propagation criterion) at there fracture tip. Following [18,19], it is assumed that the fracture width near the fracture tip follows the asymptotic solution that corresponds to a propagation of a semi-infinite hydraulic fracture (with no leak-off), which can be written as

$$w(x, z = 0) = \frac{4}{\pi} \bar{w}(x) = w_a(l - x), \quad l - \epsilon \leq x \leq l, \tag{9}$$

where  $w_a$  is the aforementioned asymptotic solution and  $\epsilon$  determines fracture tip region (one element size in numerical calculations). In the limiting cases the asymptotic solution corresponds either to the so-called viscous or toughness asymptotic solution, namely

$$w_a(s) \rightarrow \beta_m \left(\frac{\mu V}{E'}\right)^{1/3} s^{2/3}, \quad s \rightarrow \infty, \quad w_a(s) \rightarrow \sqrt{\frac{32}{\pi}} \frac{K_{Ic}}{E'} s^{1/2}, \quad s \rightarrow 0.$$

where  $\beta_m = 2^{1/3} 3^{5/6}$ ,  $s$  is the distance to the tip, and  $V$  is the velocity of the fracture front. The asymptotic solution  $w_a$  transitions from one limiting case to another as the distance from the tip and velocity of propagation change, see [20,21] for more detailed discussion about the asymptotic solution. To calculate  $w_a$ , it is possible to use either interpolated numerical solution [18] or a global approximation [19,21]. A global approximation for  $w_a$  described in [19] is used in this study.

There are two possible ways for describing the geometry of the tip region. In the first, the fracture tip remains flat (as in the original PKN model), and the fracture opening for the tip element is calculated based on the asymptotic solution for a semi-infinite fracture (9). In the second possibility, which is used in this study, a curved fracture tip (together with the asymptotic solution (9)) is utilized. This procedure is identical for the PKN and P3D geometries, and since it has been

described in [16] for the P3D fracture geometry, is omitted here. In addition, the numerical algorithm for modeling PKN fractures and P3D fractures is very similar, and is also omitted in this study.

### 2.3. Comparison with a reference solution: PKN geometry

Sections 2.1 and 2.2 describe three different approaches to model a hydraulic fracture with a PKN geometry. The first, referred to as PKN- $p_E$ , requires us to solve the lubrication Eq. (3) with the boundary condition  $\bar{w}_E$  in (6). The second, referred to as PKN- $p_R$ , consists of solving the lubrication Eq. (3) subject to the boundary condition  $\bar{w}_R$  in (6). Finally, in the third approach, referred to as the EPKN model, the governing Eq. (2) is solved together with the non-local elasticity integral Eq. (7), and using the appropriate asymptotic solution for the tip element (9). All three methods require the numerical solution of a one-dimensional problem, and are therefore computationally efficient. In order to assess the accuracy of all three approaches, the results are compared to a reference solution. The latter reference solution is calculated using a special version of an Implicit Level Set Algorithm (ILSA) [5,18], which allows us to model PKN fracture geometry in a fully planar hydraulic fracturing simulator. The ILSA solution does not rely on the assumptions made in PKN model, such as an elliptical cross-section or uniform pressure distribution in the vertical direction. At the same time, due to the complexity of the ILSA algorithm, and the fact that the whole fracture plane needs to be discretized, the ILSA solution is unable to provide comparably rapid results.

In order to compare the different hydraulic fracturing models for the PKN fracture geometry, a set of trial problem parameters is considered. This set of parameters corresponds to the laboratory experiment in [22]. The values of the parameters for the computation are  $H = 0.05$  m,  $\mu = 30.2$  Pa·s,  $\nu = 0.4$ ,  $E = 3.3$  GPa,  $Q_0 = 1.7$  mm<sup>3</sup>/s. The rock is assumed to be impermeable in all models (i.e. no leak-off). Different values of the fracture toughness in the range  $0.16 \leq K_{Ic} \leq 1.57$  MPa·m<sup>1/2</sup> are considered for comparison. Fig. 2 shows the comparison between PKN- $p_E$  (dashed red lines), PKN- $p_R$  (dashed blue lines), EPKN (dashed black lines), and the reference ILSA (solid gray lines) solutions. The top picture compares the fracture footprints at time  $t = 604$  s for three different values of fracture toughness  $K_{Ic} = \{0.47, 0.94, 1.57\}$  MPa·m<sup>1/2</sup> (squares, circles, and diamonds are used to distinguish between different values of  $K_{Ic}$ , respectively). The two pictures in the middle row show the comparison of the fracture widths and pressures at  $z = 0$  versus  $x$ , all for  $t = 604$  s, and the same three different values of fracture toughness. The bottom left picture shows the fracture length histories for all models for the same three values of  $K_{Ic}$ . Finally, the bottom right picture shows the prediction of fracture length at specified times  $t = \{200, 604, 1048\}$  s for different values of fracture toughness in the range  $0.16 \leq K_{Ic} \leq 1.57$  MPa·m<sup>1/2</sup>. Fig. 2 shows that the EPKN model is able to accurately capture the reference ILSA solution for all considered values of fracture toughness, including the curvature of the fracture tip. Both PKN- $p_E$  and PKN- $p_R$  models work well for moderate values of fracture toughness ( $K_{Ic} = 0.47$  MPa·m<sup>1/2</sup> case), when the viscous pressure drop along the fracture is comparable to the pressure boundary condition (i.e. the value of pressure at the tip). In situations when the viscous pressure drop is much smaller than the pressure at the tip (see the  $K_{Ic} = \{0.94, 1.57\}$  MPa·m<sup>1/2</sup> cases), PKN- $p_E$  and PKN- $p_R$  models are less accurate, predict constant fracture width along the length of the fracture, and are unable to capture the near-tip behavior. The comparison between the PKN- $p_E$  and PKN- $p_R$  models reveals, that the predictions of the PKN- $p_E$  model are closer to the reference solution for all parameters considered. At the same time, the level of accuracy is substantially less than that of the EPKN model.

The comparison between the three different PKN models indicates that if one needs to obtain fast and accurate predictions for the PKN fracture geometry, then the EPKN model with non-local elasticity is the appropriate choice. At the same time, as shown in [15], it is possible to utilize the PKN- $p_E$  model to obtain asymptotic solutions (which is not simple for the EPKN model), in which case no numerical calculations are needed. Fig. 2 can also be used to estimate the accuracy of the PKN- $p_E$  model and the corresponding asymptotic solutions. Finally, the PKN- $p_R$  model does not offer any advantages over the PKN- $p_E$  or EPKN model.

## 3. Comparison of toughness propagation criteria for a pseudo-3D (P3D) hydraulic fracture

### 3.1. Pseudo-3D model with local elasticity and pressure boundary condition

This section describes the classical pseudo-3D (P3D) model with symmetrical stress barriers and no leak-off, which incorporates the effect of lateral toughness by the way of a suitable boundary condition at the fracture tip (see [13] for the analysis of such model, albeit with leak-off and without lateral toughness). The P3D model under consideration assumes that the reservoir layer with height  $H$  is surrounded by two symmetric stress barriers that impose an additional confining stress  $\Delta\sigma$ , see Fig. 3. As for the PKN fracture, a fracture grows predominantly in the horizontal direction (i.e. along the  $x$  axis), but height growth in the vertical direction is also allowed. The P3D model we consider assumes the following: (i) the vertical component of the flux is negligible compared to the horizontal component, in which case the pressure is uniform along the  $z$  axis, (ii) plane strain (local) elasticity conditions apply for any vertical ( $y, z$ ) cross-section, (iii) the lateral fracture tip is vertical and its height is determined from the boundary condition. Note that the last assumption differs from the similar assumption of the classical P3D model, which states that the fracture height at the tip is equal to the reservoir height  $H$ .

The combination of plane-strain elasticity, uniform pressure in each ( $y, z$ ) plane, and toughness propagation criterion lead to the following relations analogous to (1) (see e.g. [13]):

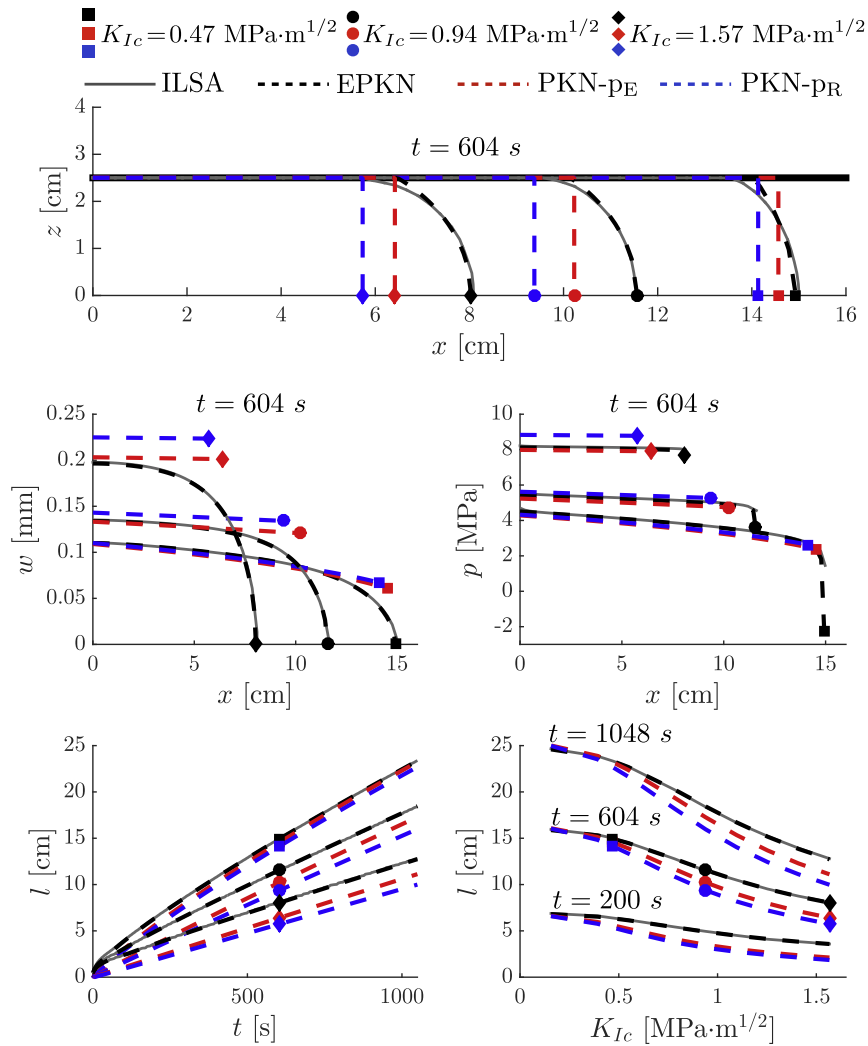


**Fig. 2.** Comparison between the predictions of the ILSA (solid gray lines), EPKN (dashed black lines), PKN-p<sub>E</sub> (dashed red lines), and PKN-p<sub>R</sub> (dashed blue lines) models for a reference set of parameters for a PKN fracture geometry. The top picture shows footprints at  $t = 604 \text{ s}$  for three different values of fracture toughness  $K_{Ic} = \{0.47, 0.94, 1.57\} \text{ MPa}\cdot\text{m}^{1/2}$  (squares, circles, and diamonds, respectively). The middle row pictures compare the fracture width and fluid pressure variations at  $z = 0$  versus  $x$  at  $t = 604 \text{ s}$  for the same three values of fracture toughness. The bottom left picture plots the time histories of the fracture length for the three considered values of  $K_{Ic}$ . The bottom right picture indicates the variation of fracture length versus  $K_{Ic}$ , measured at different time instants  $t = \{200, 604, 1048\} \text{ s}$ . (For interpretation of the references to color in this figure legend, the reader is referred to the web version of this article.)

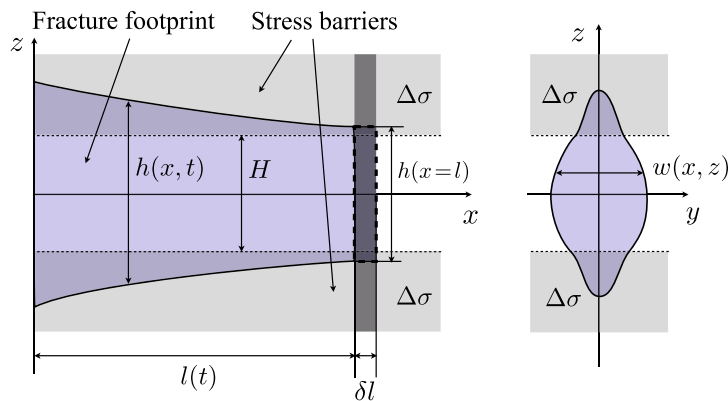


**Fig. 3.** Schematics of a P3D fracture. The rectangle at the fracture tip with dashed borders indicates incremental fracture growth. Dark shaded area indicates area in the rock where additional elastic energy is introduced due to incremental fracture growth (according to plane strain (local) elasticity assumption).

$$w(x, z) = \frac{2}{E'} \sqrt{\frac{2}{\pi h}} K_{Ic} \chi + \frac{4\Delta\sigma}{\pi E'} \left\{ -z \ln \left| \frac{H\chi + 2z\psi}{H\chi - 2z\psi} \right| + \frac{H}{2} \ln \left| \frac{\chi + \psi}{\chi - \psi} \right| \right\}, \tag{10}$$

$$\bar{w}(x) = \hat{w}(h, K_{Ic}) \equiv \frac{1}{H} \int_{-h/2}^{h/2} w dz = \frac{H}{E'} \left( \sqrt{\frac{\pi}{2H}} K_{Ic} \left( \frac{h}{H} \right)^{3/2} + \Delta\sigma \sqrt{\frac{h^2}{H^2} - 1} \right), \tag{11}$$

$$p(x) = \hat{p}(h, K_{Ic}) = \sqrt{\frac{2}{\pi h}} K_{Ic} + \Delta\sigma \left[ 1 - \frac{2}{\pi} \arcsin \left( \frac{h}{H} \right) \right], \tag{12}$$

where  $w(x, z)$  is the fracture width,  $\Delta\sigma$  is the amplitude of the stress barrier,  $h$  denotes fracture height (see Fig. 3),  $p$  is the fluid pressure,  $\chi = \sqrt{h^2 - 4z^2}$ ,  $\psi = \sqrt{h^2 - H^2}$ ,  $E' = E/(1 - \nu^2)$  is the plane strain Young's modulus, while  $K_{Ic}$  is the fracture toughness. Note that  $\hat{w}$  and  $\hat{p}$  are introduced here as functions of  $h$  and  $K_{Ic}$ , in which case other parameters such as  $E'$ ,  $\Delta\sigma$ , and  $H$  are treated as constants. Also note that the fluid pressure  $p(x)$  and average fracture width  $\bar{w}(x)$  depend on  $x$  through the spatial variation of the fracture height  $h$ .

The lubrication equation for a P3D fracture is very similar to (2) and (3), and reads

$$\frac{\partial \bar{w}}{\partial t} + \frac{\partial \bar{q}_x}{\partial x} = \frac{Q_0}{H} \delta(x), \quad \bar{q}_x = -\frac{1}{H\mu'} \frac{\partial p}{\partial x} \int_{-h/2}^{h/2} w^3 dz, \tag{13}$$

where  $\mu' = 12\mu$  is the scaled fluid viscosity, while  $Q_0$  is the total fluid volume pumped into the fracture per unit time (the source is located at  $x = 0$ ). Note that Eq. (11) can be inverted (numerically) to produce the function  $h(\bar{w})$ , which can be substituted into (10) and (12) to find the fracture width and the pressure in terms of the material properties and  $\bar{w}$ . In this case, the average flux in Eq. (13) becomes a function only of the effective width  $\bar{w}$ , and the lubrication equation in (13) can be solved for  $\bar{w}$ , once the boundary condition at the tip is specified (which is described below). The details of the numerical scheme are omitted for brevity.

The classical boundary condition for the P3D model,  $\bar{w}(l) = 0$ , is unable to capture the effect of lateral fracture toughness. In order to obtain a pressure boundary condition for the P3D fracture geometry that is based on the energy considerations, this paragraph aims to extend the derivation in [15] from PKN to P3D fractures, and to obtain an analog of (4). The elastic energy per unit length of a P3D fracture is equal to the work of the fluid pressure required to open a pre-existing fracture with length  $h$ , i.e.

$$U_{ps} = \int_0^{\bar{w}} p d(H\bar{w}) = H \int_H^h \hat{p}(\hat{h}, 0) \frac{\partial \hat{w}(\hat{h}, 0)}{\partial \hat{h}} d\hat{h} + H \int_0^{K_{Ic}} \hat{p}(h, K_I) \frac{\partial \hat{w}(h, K_I)}{\partial K_{Ic}} dK_I. \tag{14}$$

It is noted here that  $\hat{w}(h, K_{Ic})$  and  $\hat{p}(h, K_{Ic})$  are given respectively in (11) and (12) and are treated as functions of two variables  $h$  and  $K_{Ic}$ , in which case  $\partial \hat{w}(\hat{h}, 0)/\partial \hat{h}$  denotes the partial derivative with respect to the first argument (i.e.  $h$ ) that is evaluated at  $h = \hat{h}$  and  $K_{Ic} = 0$ . The same applies to the pressure  $p$ . The first integral in (14) calculates the work needed to “grow” the fracture to the length  $h$  with no fracture toughness, and the second integral calculates the work required to further open the fracture at the fixed length  $h$  (until stress intensity factor reaches its critical value, i.e.  $K_I = K_{Ic}$ ). Note that the same elastic energy integral (14) can be calculated assuming that the fracture breaks the rock while growing from  $H$  to  $h$ , in which case the corresponding fracture energy needs to be included. If one considers the energy balance associated with the incremental fracture growth in the  $x$  direction by  $\delta l$ , then

$$p(l)H\bar{w}(l)\delta l = U_{ps}(l)\delta l + G_c h(l)\delta l, \tag{15}$$

where the first term represents the work done by the fluid pressure to open the fracture (at constant pressure), the second term is the increase in the strain energy in the rock, and the third term accounts for the energy required to fracture the rock, where  $G_c$  is the fracture energy per unit area, see Fig. 3. The combination of (14) and (15) with the use of (11) and (12) allows us to find

$$\begin{aligned} G_c &= -\frac{U_{ps}(l) - p(l)H\bar{w}(l)}{h(l)} = \frac{H}{h(l)} \int_0^{p(l)} \bar{w} dp = \frac{H}{h(l)} \int_H^{h(l)} \hat{w}(\hat{h}, 0) \frac{\partial \hat{p}(\hat{h}, 0)}{\partial \hat{h}} d\hat{h} + \frac{H}{h(l)} \int_0^{K_{Ic}} \hat{w}(h, K_I) \frac{\partial \hat{p}(h, K_I)}{\partial K_{Ic}} dK_I \\ &= \frac{2\Delta\sigma^2 H^2}{\pi E' h(l)} \ln \left( \frac{h(l)}{H} \right) + \frac{K_{Ic}^2}{2E'} + \sqrt{\frac{2}{\pi h(l)} \frac{\Delta\sigma K_{Ic} H^2}{E' h(l)} \sqrt{\left( \frac{h(l)}{H} \right)^2 - 1}}. \end{aligned} \tag{16}$$

Since the fracture energy per unit area is  $G_c = K_{Ic}^2/E'$ , then the latter equation can be simplified to

$$\frac{\lambda \mathcal{K}_{P3D}^2}{8} = \ln(\lambda) + \frac{1}{2} \mathcal{K}_{P3D} \sqrt{\lambda - \frac{1}{\lambda}}, \tag{17}$$

where

$$\mathcal{K}_{P3D} = \sqrt{\frac{2\pi K_{Ic}}{H \Delta\sigma}}, \quad \lambda = \frac{h(l)}{H}. \quad (18)$$

The numerical inversion of (17) allows us to find  $h(l)$ , which can be substituted to (11) to obtain the boundary condition in the form  $p_E(l) = p(h(l))$  or  $\bar{w}_E(l) = \bar{w}(h(l))$  for a P3D fracture. It is interesting to note that for small values of  $\mathcal{K}_{P3D}$ , the boundary condition reduces to

$$\frac{p_E(l)}{\Delta\sigma} = \frac{\sqrt{2}}{\pi} \mathcal{K}_{P3D} + O(\mathcal{K}_{P3D}^3), \quad \lambda = 1 + \frac{(\sqrt{2}-1)^2}{2^3} \mathcal{K}_{P3D}^2 + O(\mathcal{K}_{P3D}^4), \quad \mathcal{K}_{P3D} \ll 1,$$

which, in the limit, becomes identical to that for a PKN fracture (4). Also, Eq. (17) has a unique solution only until  $\mathcal{K}_{P3D} \approx 3.29$ , which corresponds to a maximum scaled height growth  $\lambda \approx 1.98$ . There is no solution for larger values of  $\mathcal{K}_{P3D}$ , since this corresponds to an unstable height growth regime at the fracture tip. This unstable height growth is reached when the pressure (12) reaches its maximum value as a function of height [13]. As a result, the P3D model with the boundary condition stemming from (17) is certainly unable to provide a solution for  $\mathcal{K}_{P3D} > 3.29$ . For completeness, the pressure boundary condition calculated based on the pressure of the radial solution is considered as well, namely

$$p_R(l) = \sqrt{\frac{\pi}{2H}} K_{Ic}. \quad (19)$$

which is identical to (5). The combination of (19) and (12) allows us to determine  $h(l)$ , which consequently leads to  $\bar{w}_R(l) = \bar{w}(h(l))$ . Note that, with the reference to (18), the maximum allowed value of fracture toughness, and the corresponding value of the height at the tip, can be deduced as  $\mathcal{K}_{P3D} \approx 2.48$ , and  $\lambda \approx 2.94$ . In other words, the P3D model with the boundary condition (19) is unable to provide a solution for  $\mathcal{K}_{P3D} > 2.48$  since unstable height growth happens at the tip. It should be noted here that the unstable height growth can even occur in situations when  $\mathcal{K}_{P3D}$  is below the critical value, since the prediction of the fracture height at the wellbore is larger than that at the tip.

### 3.2. Comparison with a reference solution: P3D geometry

This section aims to compare different methods that can be used to include the effect of lateral fracture toughness into the P3D model. The first method, referred here as P3D- $p_E$ , consists of solving the lubrication Eq. (13) together with (10)–(12) and the boundary condition determined from (17)–(18). In the second approach, called P3D- $p_R$ , the lubrication Eq. (13) is solved in conjunction with (10)–(12) and the boundary condition (19). The P3D model with non-local elasticity used here for comparison, named EP3D, has been described in [16]. Note that a version with the asymptotic solution (9), described in [19] is used. All P3D- $p_E$ , P3D- $p_R$ , and EP3D models require the numerical solution of a one-dimensional equation, and therefore are all computationally efficient. The aforementioned models are compared to a reference solution, calculated using an Implicit Level Set Algorithm (ILSA) [18]. The latter is a fully planar hydraulic fracturing simulator that does not rely on any of the assumptions of the P3D model.

As for the PKN fracture geometry, a set of reference parameters that corresponds to the laboratory experiment in [22] is used. The values of the parameters are  $H = 0.05$  m,  $\mu = 30.2$  Pa·s,  $\nu = 0.4$ ,  $E = 3.3$  GPa,  $Q_0 = 1.7$  mm<sup>3</sup>/s, and  $\Delta\sigma = 4.3$  MPa, while the rock is assumed impermeable in all models (i.e. no leak-off). Different values of fracture toughness in the range  $0.16 \leq K_{Ic} \leq 1.57$  MPa·m<sup>1/2</sup> are considered for comparison. Fig. 4 is an analog of Fig. 2, but for the P3D geometry, and shows the comparison between P3D- $p_E$  (dashed red lines), P3D- $p_R$  (dashed blue lines), EP3D (dashed black lines), and the reference ILSA (solid gray lines) solutions. The top picture compares the fracture footprints at time  $t = 604$  s for three different values of fracture toughness  $K_{Ic} = \{0.47, 0.94, 1.57\}$  MPa·m<sup>1/2</sup> (squares, circles, and diamonds are used to distinguish between different values of  $K_{Ic}$ , respectively). The two pictures in the middle row show the comparison of the fracture widths and pressures at  $z = 0$  versus  $x$ , all for  $t = 604$  s, and the same three different values of fracture toughness. The bottom left picture shows the fracture length histories for all models for the same three values of  $K_{Ic}$  as well. Finally, the bottom right picture shows prediction of fracture length at specified times  $t = \{200, 604, 1048\}$  s for different values of fracture toughness in the range  $0.16 \leq K_{Ic} \leq 1.57$  MPa·m<sup>1/2</sup>. Note that the P3D- $p_E$  results are plotted only for  $K_{Ic} = \{0.47, 0.94\}$  MPa·m<sup>1/2</sup>, while P3D- $p_R$  results are shown only for  $K_{Ic} = 0.47$  MPa·m<sup>1/2</sup>. The reason is that for the missing  $K_{Ic}$  values the corresponding P3D models with local elasticity reach unstable height growth regimes (or very close to these regimes, in which case the accuracy is low). Fig. 4 shows that the EP3D model is able to accurately capture the reference ILSA solution for all considered values of fracture toughness, and does not exhibit an unstable height growth regime. Both the P3D- $p_E$  and P3D- $p_R$  models work acceptably well for moderate values of fracture toughness (i.e.  $K_{Ic} = 0.47$  MPa·m<sup>1/2</sup> case), when the viscous pressure drop along the fracture is comparable to the pressure boundary condition (i.e. the value of pressure at the tip). Both the P3D- $p_E$  and P3D- $p_R$  models experience a rapid accuracy decay for increasing values of the fracture toughness, and eventually reach an unstable height growth regime. As was the case for the PKN fracture geometry, the energy-based boundary condition provides better results than the P3D- $p_R$  model. Note that the fracture height growth prediction of the P3D- $p_E$  model for  $K_{Ic} = 0.94$  MPa·m<sup>1/2</sup> is accurate, despite the fracture length is noticeably underestimated. This is related to the fact that the local elasticity assumption provides a good approximation near the wellbore, whereby the fracture height is determined solely by the fluid pressure at

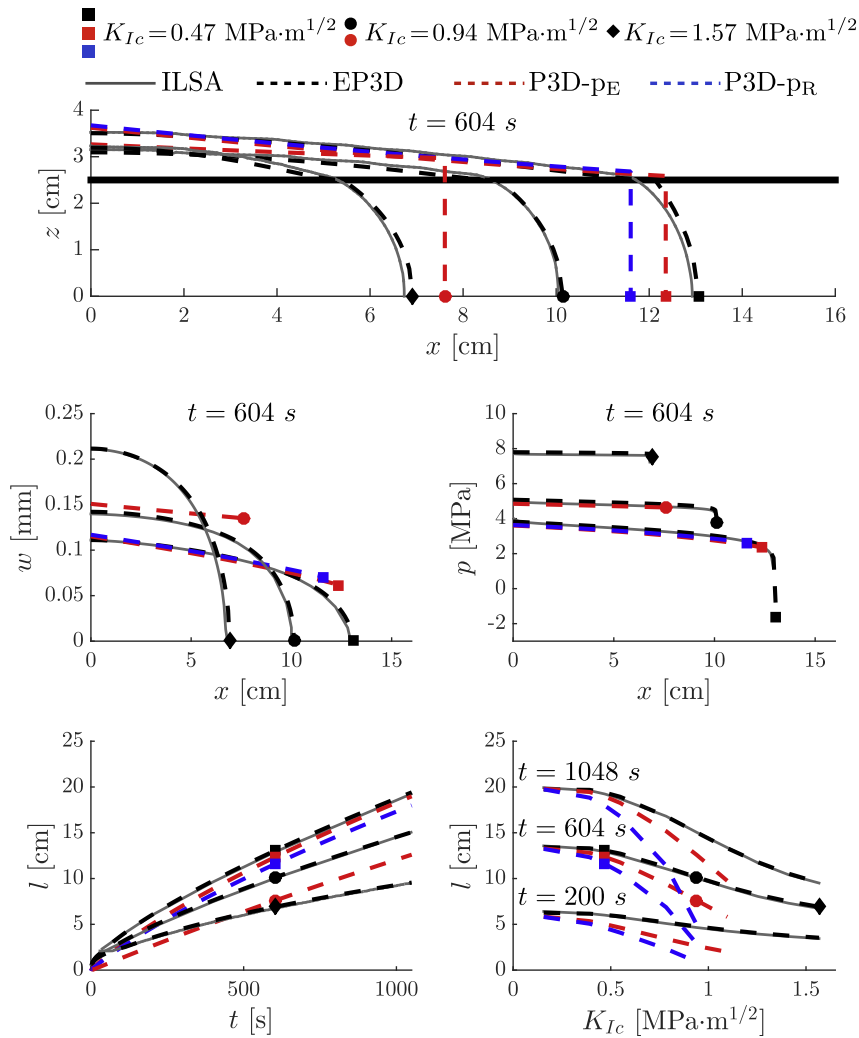


**Fig. 4.** Comparison between the predictions of the ILSA (solid gray lines), EP3D (dashed black lines), P3D-p<sub>E</sub> (dashed red lines), and P3D-p<sub>R</sub> (dashed blue lines) models for a reference set of parameters for a P3D fracture geometry. The top picture shows footprints at  $t = 604$  s for three different values of fracture toughness  $K_{Ic} = \{0.47, 0.94, 1.57\}$  MPa·m<sup>1/2</sup> (squares, circles, and diamonds, respectively). The middle row pictures compare fracture width and fluid pressure variations at  $z = 0$  versus  $x$  at  $t = 604$  s for the same three values of fracture toughness. The bottom left picture plots the time histories of the fracture length for the three considered values of  $K_{Ic}$ . The bottom right picture indicates the variation of the fracture length versus  $K_{Ic}$ , measured at different time instants  $t = \{200, 604, 1048\}$  s. (For interpretation of the references to color in this figure legend, the reader is referred to the web version of this article.)

the wellbore, which is captured accurately by the P3D-p<sub>E</sub> model. Despite the fracture height growth is captured accurately at the wellbore, its variation along the fracture is not accurate, which produces an influence on the length accuracy due to a fracture volume conservation.

Comparison between the results shown in Figs. 2 and 4 clearly indicates that the reduced models featuring the non-local elasticity (i.e. EPKN and EP3D) are able to provide consistently accurate results for both the PKN and P3D fracture geometries. The model with local elasticity and the energy-based boundary condition is capable of providing reasonably accurate results for the PKN fracture geometry, but quickly becomes inaccurate (and eventually unstable) for the P3D geometry for increasing values of fracture toughness. The model with the local elasticity and boundary condition originating from matching the pressure for a radial fracture is consistently less accurate than its counterpart with the energy-based boundary condition. It should be noted here that one can potentially design a boundary condition for a P3D model with local elasticity, so that the length versus  $K_{Ic}$  curves in Fig. 4 match. In this case, however, the fracture height and width will unlikely be matched in the toughness regime of propagation. In the latter regime, the pressure is nearly constant along the fracture, which implies that the fracture width and height are constant as well. In this situation, one tries to approximate a fracture with smoothly varying footprint and width by a model in which the footprint is rectangular and the fracture width is constant. In addition, the use of local elasticity inevitably leads to an unstable height growth condition for large values of fracture toughness. This

makes a P3D model with local elasticity and any boundary condition at the tip (that aims to capture the effect of fracture toughness) less suitable than the EP3D model with non-local elasticity, which is stable, and is able to capture smooth footprint and width variations.

#### 4. Summary

This paper compares different methods that can be employed to capture the effect of lateral fracture toughness for PKN and P3D hydraulic fractures. In the first two methods, the classical PKN and P3D models are augmented by a special pressure boundary condition, which depends on the fracture toughness. In particular, the value of the pressure at the tip can either be calculated based on the energetic considerations, or taken from the solution for a radial fracture (which is equivalent to “stitching” the radial fracture tip to the rest of the fracture). The third method utilizes a qualitatively different approach, in which a plane strain (or local) elasticity assumption is replaced by a suitable non-local elasticity equation. In the latter case, the effect of the lateral fracture toughness is captured by using an asymptotic solution for the tip element, which is consistent with the standard linear elastic fracture mechanics fracture propagation criterion. All the aforementioned reduced models are compared to a reference solution that is calculated using a fully planar hydraulic fracturing simulator. The results demonstrate that the reduced models with non-local elasticity are remarkably accurate for a wide range of fracture toughness values for both PKN and P3D fracture geometries. At the same time, the model with local elasticity and an energy-based tip boundary condition produces reasonably accurate results for a PKN fracture geometry, while it becomes inaccurate, and eventually unstable, for relatively large values of fracture toughness for the P3D fracture geometry. The model with local elasticity and the boundary condition originating from “stitching” a radial fracture to the tip showed the worst performance among all three considered approaches, while, at the same time, is able to provide relatively accurate results for moderate values of fracture toughness.

#### Acknowledgements

The support of the British Columbia Oil and Gas Commission and the NSERC discovery grants program is gratefully acknowledged.

#### References

- [1] Khristianovic S, Zheltov Y. Formation of vertical fractures by means of highly viscous fluids. *Proc 4th world petroleum congress*, vol. 2. p. 579–86.
- [2] Gordeliy E, Detournay E. A fixed grid algorithm for simulating the propagation of a shallow hydraulic fracture with a fluid lag. *Int J Numer Anal Methods Geomech* 2011;35:602–29.
- [3] Savitski A, Detournay E. Similarity solution of a penny-shaped fluid-driven fracture in a zero-toughness linear elastic solid. *CR Acad Sci II B* 2001;329:255–62.
- [4] Vandamme L, Curran J. A three-dimensional hydraulic fracturing simulator. *Int J Numer Methods Engng* 1989;28:909–27.
- [5] Peirce A, Detournay E. An implicit level set method for modeling hydraulically driven fractures. *Comput Methods Appl Mech Engng* 2008;197:2858–85.
- [6] Peirce A, Bungler A. Interference fracturing: non-uniform distributions of perforation clusters that promote simultaneous growth of multiple hydraulic fractures. *SPE* 172500.
- [7] Wu R, Kresse O, Weng X, Cohen C-E, Gu H. Modeling of interaction of hydraulic fractures in complex fracture networks. In: *Society of petroleum engineers*, SPE 152052.
- [8] Perkins T, Kern L. Widths of hydraulic fractures. *J Petrol Tech Trans AIME* 1961;937–49.
- [9] Nordgren R. Propagation of vertical hydraulic fractures. *Soc Petrol Eng J* 1972;12:306–14.
- [10] ID IP, Carroll H. Three-dimensional hydraulic fracture propagation in the presence of stress variation. In: *Proceedings of the SPE/DOE/GRI unconventional gas recovery symposium*, SPE/DOE 10849. p. 870–8.
- [11] ID IP, Carroll H. Numerical solution for height and elongated hydraulic fractures. In: *Proceedings of the SPE/DOE low permeability reservoir symposium*, Denver. SPE 11627. p. 249–56.
- [12] Settari A, Cleary M. Development and testing of a pseudo-three-dimensional model of hydraulic fracture geometry (p3dh). In: *Proceedings of the 6th SPE symposium on reservoir simulation of the society of petroleum engineers*, SPE 10505. p. 185–214.
- [13] Adachi JI, Detournay E, Peirce AP. An analysis of classical pseudo-3D model for hydraulic fracture with equilibrium height growth across stress barriers. *Int J Rock Mech Min Sci* 2010;47:625–39.
- [14] Nolte K. Fracturing-pressure analysis for nonideal behavior. *J Petrol Technol* 1991;43:210–8.
- [15] Sarvaramini E, Garagash D. Breakdown of a pressurized fingerlike crack in a permeable solid. *J Appl Mech* 2015;82:061006.
- [16] Dontsov E, Peirce A. An enhanced pseudo-3D model for hydraulic fracturing accounting for viscous height growth, non-local elasticity, and lateral toughness. *Engng Fract Mech* 2015;142:116–39.
- [17] Adachi J, Peirce A. Asymptotic analysis of an elasticity equation for a finger-like hydraulic fracture. *J Elasticity* 2008;90:43–69.
- [18] Peirce A. Modeling multi-scale processes in hydraulic fracture propagation using the implicit level set algorithm. *Comput Methods Appl Mech Engng* 2015;283:881–908.
- [19] Dontsov E, Peirce A. Incorporating viscous, toughness, and intermediate regimes of propagation into enhanced pseudo-3D model. *San Francisco (CA): American Rock Mechanics Association*; 2015.
- [20] Garagash D, Detournay E, Adachi J. Multiscale tip asymptotics in hydraulic fracture with leak-off. *J Fluid Mech* 2011;669:260–97.
- [21] Dontsov E, Peirce A. A non-singular integral equation formulation to analyze multiscale behaviour in semi-infinite hydraulic fractures. *J Fluid Mech* 2015;781:R1.
- [22] Jeffrey R, Bungler A. A detailed comparison of experimental and numerical data on hydraulic fracture height growth through stress contrasts. In: *Society of petroleum engineers*, SPE 106030.